ChemComm

Efficient Large Guanidinium Mixed Perovskite Solar Cells with Enhanced Photovoltage and Low Energy Losses

Journal:	*ChemComm*
Manuscript ID	CC-COM-01-2019-000016.R2
Article Type:	Communication

Journal Name

COMMUNICATION

Efficient Large Guanidinium Mixed Perovskite Solar Cells with Enhanced Photovoltage and Low Energy Losses

Shengfan Wu,[a] Zhen Li,[a] Jie Zhang,[a] Tiantian Liu,[a] Zonglong Zhu,*[a] and Alex K.-Y. Jen*[ab]

Received 00th January 20xx,
Accepted 00th January 20xx

DOI: 10.1039/x0xx00000x

www.rsc.org/

We present a strategy for suppressing open-circuit voltage (V_{oc}) loss of perovskite solar cells by incorporating large guanidinium cation (Gua^+) into perovskite lattice, leading to a significantly improved V_{oc} of 1.19 V and an impressive power conversion efficiency of >21%. Our results manifest the critical role of Gua in passivating defects and highlight the importance of compositional engineering in promoting the performance of perovskites.

Solution processable organic-inorganic lead halide perovskite solar cells (PVSCs) have attracted enormous attention from both industry and academia as a promising photovoltaic technology for renewable energy generations.[1, 2] Very recently, a PVSC with certified power conversion efficiency (PCE) has already reached 23.7%,[3] which is on par with the performance of several existing inorganic photovoltaic technologies. Although PVSCs has developed so rapidly, it becomes more and more challenging to further improve efficiency as it has already approached theoretical limit. For state-of-the-art PVSCs, the reported short-circuit current densities (J_{SC}) have reached 92% of their theoretical maximum while the V_{oc} and fill factors (FF) are still less than 90% of Shockley−Queisser limit.

Given that any non-radiative losses can potentially narrow the quasi-Fermi level splitting (QFLS),[4] large number of defects within perovskite or at its grain boundaries and interfaces acted primarily as nonradiative centres contributing to the most significant voltage loss ($V_{oc,\ loss} = E_g/q - V_{oc}$).[5] The $V_{oc,\ loss}$ plotted as a function of PCE from some recently reported single-junction PVSCs based on n-i-p configuration are shown in **Fig. S1**. To tackle voltage loss issues, composition engineering, surface treatments/passivation and interfacial modifications are the most commonly used methods to reduce the defect states of halide perovskites.[6-9] Among of them, composition engineering for halide perovskite has been proven to be a highly effective strategy for achieving efficient PVSCs with low voltage loss since it can improve the quality of perovskite film thus reduce the defects in grain boundaries and on surfaces.

Several research groups have recently reported that the defects in perovskite films can be effectively modulated by employing additives in the precursor solutions. Saliba *et al*. demonstrated that the incorporation of rubidium iodide (RbI) can improve the photoluminescent quantum yield (PLQY) of Cs-FA-MA based perovskite from 2.4 to 3.6%, correspondingly, a high V_{oc} of 1.24 V could be obtained.[10] More recently, Son *et al*. found that the addition of potassium iodide in perovskite can eliminate the hysteresis of PVSCs by preventing the formation of iodide Frenkel defects, compared to other alkali metal iodides.[11]

Organic halide salts such as butyl ammonium iodide, phenylethyl ammonium iodide, have also been used to reduce defect density of perovskite films.[12-15] However, most of the organic halide salts with large size would result in Ruddlesden–Popper layered perovskites, leading to quantum confinement effect that reduces the J_{SC} of devices. In addition to alkali halides and 2D organic cations, highly symmetric guanidinium cation (Gua^+) with an ionic radii of 278 pm has also been reported to enhance the photovoltaic performance in $MAPbI_3$ based PVSCs by forming a highly stable 3D crystalline structure.[16-20] Moreover, we have recently found that Gua alloyed perovskite possess enhanced defect tolerance and phase stability for large bandgap perovskites.[19]

In this work, large Gua cation was incorporated into $Cs_{0.1}(FA_{0.83}MA_{0.17})_{0.9}Pb(I_{0.83}Br_{0.17})_3$ perovskites to form CsGuaFAMA mixed cation perovskites. The remarkably prolonged carrier lifetime, sharper Urbach tail and lower trap density of states (tDOS) demonstrated the strong passivation effect of Gua on the defects in bulk perovskite. As a result, the 10% Gua (molar ratio) based PVSCs yield a champion PCE of 21.12%. More importantly, an impressive V_{oc} of 1.19 V can be

[a] Department of Chemistry, City University of Hong Kong, Kowloon, 999077, Hong Kong. Email: zonglzhu@cityu.edu.hk; alexjen@cityu.edu.hk
[b] Department of Materials Science and Engineering, City University of Hong Kong, Kowloon, 999077, Hong Kong
Electronic Supplementary Information (ESI) available: [details of any supplementary information available should be included here]. See DOI: 10.1039/x0xx00000x

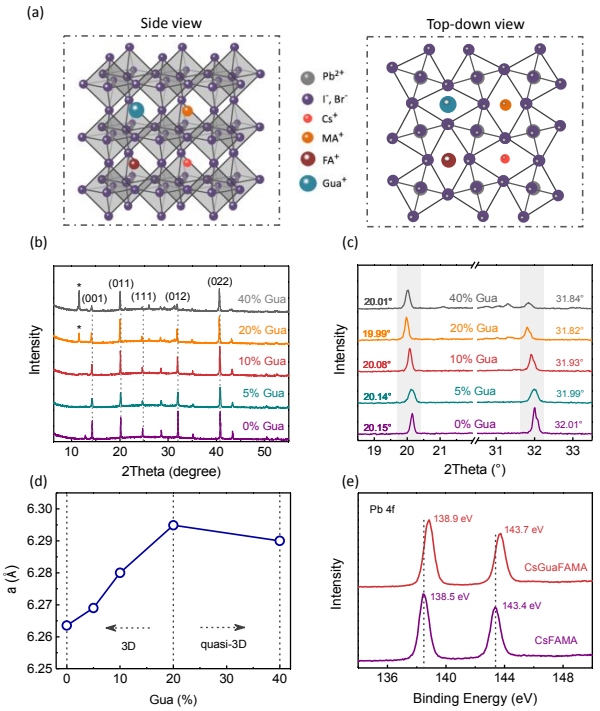

Fig. 1 (a) Side and top-down view of the crystal structure of CsGuaFAMA mixed cation perovskites. (b) X-ray diffraction (XRD) measurements of $Gua_x(CsFAMA)_{1-x}$ perovskite films and (c) magnification of the XRD peaks at (011) and (012). (d) Lattice parameter variation *a* of the mixed cation perovskite unit cell. (e) High-resolution XPS spectra of Pb 4f.

achieved with the $V_{oc,\ loss}$ of merely 420 mV. Our result suggests that Gua^+ can function as a unique alternative cation to suppress the formation of lattice defects and be generally applicable for other perovskite-based optoelectronic devices.

$Cs_{0.1}(FA_{0.83}MA_{0.17})_{0.9}Pb(I_{0.83}Br_{0.17})_3$ (denoted as CsFAMA) is used as the reference to investigate the structural, optical, and electrical properties of Gua based perovskites. Considering the complex nature of Gua-incorporated films, the molar ratio (x) of Gua to $Cs_{0.1}(FA_{0.83}MA_{0.17})_{0.9}Pb(I_{0.83}Br_{0.17})_3$ is used to indicate the different perovskite films. **Fig. 1a** presents the proposed crystal structures of the mixed perovskite. To gain more insight of the arrangement of Gua in perovskite crystal structure, we performed X-ray diffraction (XRD) measurements to investigate the phase and crystal information. **Fig. 1b** shows the diffraction patterns of the samples containing different molar ratio of Gua and it is noted that a small peak at 12.7° is observed for the pristine film (0% Gua), which is originated from PbI_2 in perovskite. Interestingly, upon incorporation of Gua, the intensity of diffraction peak gradually decreased while still kept 3D perovskite phase. However, a new diffraction peak at lower angle around 11.31° occurred for 20% and 40% Gua, indicating the formation of 1D $GuaPbI_3$ phase.[21] **Fig. 1c** displays the zoomed-in region corresponding to (011) and (012) lattice planes. An obvious left shift of the peaks was observed when the ratio of Gua was increased. Considering the ionic radius (*r*) of Gua is 278 pm, being larger than that of FA^+ (253 pm), it is possible that partial substitution by Gua have generated lattice expansion. To verify this hypothesis, lattice constant *a* was calculated. As plotted in **Fig. 1d**, *a* is gradually increased with increasing the concentration of Gua, proving that Gua has inserted into the perovskite lattice.[18] The average crystallite size was also calculated by *Debye–Scherrer* equation and the results are summarized in **Table S1**.

The surface electronic states of the perovskite films were investigated through X-ray photoemission spectroscopy (XPS). As shown in **Fig. 1e**, high-resolution spectra of Pb 4f for pristine film exhibit two characteristic peaks at 138.5 eV and 143.4 eV, which are shifted to 138.9 eV and 143.7 eV respectively for 10% Gua. Similarly, C 1s peaks also right shifted to higher binding energy (**Fig. S2**), which are likely resulting from different atomic environments or coordination strengths between Gua and FA/MA/Cs[22]. However, the shift of N 1s peak might be resulted from the background noise when compared with N 1s peak of 1D $GuaPbI_3$.[18] Additionally, the morphology of these perovskite films were studied through scanning electron microscopy (SEM) and atomic force microscopy (AFM), as shown in **Fig. S3 and S4**. We found that there are no clear differences between the perovskite films, indicating that the film morphology was not obviously affected by Gua.

Fig 2a and **b** display the photograph and UV-vis absorption spectra of the perovskite films with different content of Gua, respectively. A color change of the films from black (0% Gua) to brown (40% Gua) is observed, which can be attributed to the reduced absorption in visible region. All of the samples demonstrated similar band edge at around 770 nm. Specifically, the band gaps of 0% and 10% Gua (denoted as CsGuaFAMA hereafter) mixed perovskite films were calculated to be 1.62 eV and 1.61 eV, respectively (see **Fig. S5**), suggesting Gua has negligible effect on bandgap. Steady state photoluminescence (PL) were also employed to study charge dynamics of these perovskite films, as shown in **Fig. 2c**. It can be seen that 10% Gua achieved highest PL intensity and then gradually decreased when the concentration of Gua is over 10%, which indicate that a small amount of Gua can passivate the defects in perovskite films. However, the PL intensity decreased while overdose of Gua is incorporated, which might be attributed to the formation of 1D $GuaPbI_3$ that has lower PLQY. By comparing PL spectra, it is noticed that there was a gradual red shift and broaden of FWHM for 20% and 40% Gua (**Fig. S6**). This redshift is probably related to slight phase segregation changing from homogeneously mixed halide anions to bromide- and

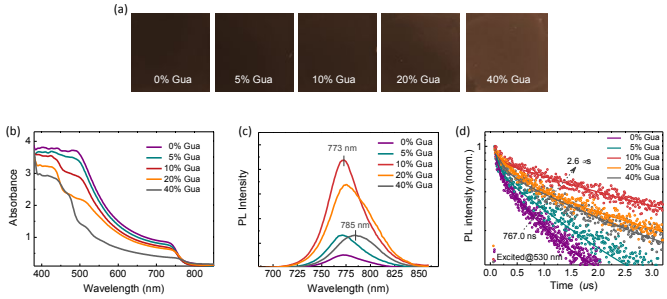

Fig. 2 (a) Photographs of $Gua_x(CsFAMA)_{1-x}$ perovskite films containing different fraction of Gua. (b) UV-vis spectra, (c) photoluminescence and (d) time-resolved photoluminescence (TRPL) spectra of the solid perovskite films with different Gua/CsFAMA ratio.

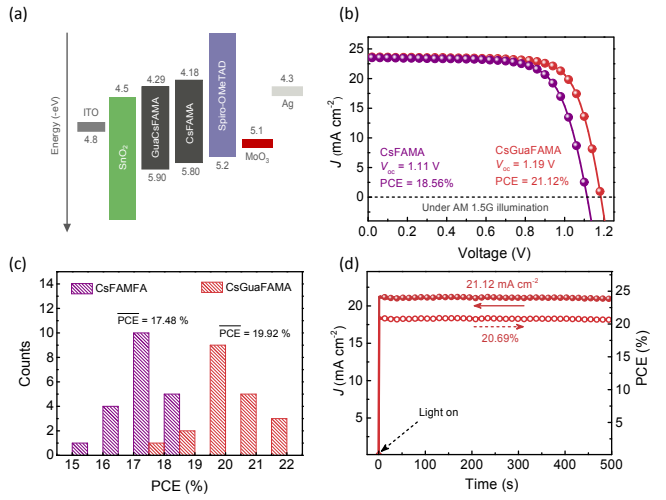

Fig. 3 (a) Energy level diagrams for different materials. (b) current density–voltage (*J–V*) curves. (c) PCE distribution of PVSCs. (d) steady out of the champion device.

iodide-rich perovskite phases at high concentration of Gua.[23]

Charge carrier kinetics of these perovskite films were characterized through time-resolved photoluminescence (TRPL) spectroscopy. As shown in **Fig. 2d**, all TRPL spectra exhibited typical bi-exponential decay behaviour and the PL decay times were fitted by bi-exponential function of time (*t*) (see ESI†). The average carrier lifetime (τ_{ave}) and the related fitting parameters are summarized in **Table S2**. The sample without Gua showed an τ_{ave} of 767.00 ns, then increased to 1.22 *u*s, 2.66 *u*s, 1.84 *u*s and 1.30 *u*s, respectively, when the Gua concertation was increased to 5%, 10%, 20% and 40%. It is reported that the increase of charge carrier lifetimes is attributed to the rapid reorientation through electron-rotor interaction of Gua in the A-site.[17] These remarkably improved PL intensity and lifetime indicated that the bi-molecular radiative recombination was gradually enhanced by embedding larger Gua cation into perovskite lattice, which is consistent with the previous reports.[17, 18, 24]

The photovoltaic performance of Gua incorporated PVSCs were examined by fabricating the regular n-i-p planar photovoltaic devices. Since it is important to select proper hole- and electron-transporting materials with compatible valance band maximum (VBM) and conduction band minimum (CBM) to perovskites, ultraviolet photoelectron spectroscopy (UPS) was carried out to measure the VBM and CBM of perovskite films (**Fig. S7**). The calculated energy levels of perovskites were provided in **Fig. 3a**, where SnO_2 and spiro-OMeTAD were accordingly chose as the ETL and HTL to form favourable cascade charge transport. The energy level alignments of the materials are depicted in **Fig. 3a** and the best current density-voltage (*J-V*) curves (measured under AM 1.5 G irradiation at 100 mW cm^{-2}) of the studied PVSCs were illustrated in **Fig. 3b**. The $Cs_{0.1}(FA_{0.83}MA_{0.17})_{0.9}Pb(I_{0.83}Br_{0.17})_3$ based PVSC showed a decent PCE of 18.56% with a short current density (J_{sc}) of 23.55 mA cm^{-2}, a V_{oc} of 1.11 V and a fill factor (*FF*) of 0.71. Whereas, 10% Gua based perovskite achieved a significantly enhanced V_{oc} of 1.19 V with a J_{sc} of 23.66 mA cm^{-2} and *FF* of 0.75, leading to a champion PCE of 21.12%. It is noted that the $V_{oc,\ loss}$ of 10% Gua is only 420 mV, which is among the lowest voltage loss in the PVSCs with E_g around 1.60 eV. On the contrary, the voltage loss for reference device is as high as 500 mV. Since planar PVSCs usually suffer from hysteresis, the *J-V* curves with forward and reverse scan were compared in **Fig. S8** and it is found that there is no obvious difference in hysteresis behavior for 10% Gua based device. All the device performance is summarized in **Table S3** and the *J-V* curves for other ratios of Gua are also provided in **Fig. S9**.

The PCE statistics of total 20 devices of each regular PVSC with 0% and 10% GUA were demonstrated in **Fig. 3c**. It is found that the average PCE of 10% Gua based PVSCs was remarkably enhanced from 17.48% to 19.92% with good reproducibility. The stabilized power output of CsGuaFAMA cell was measure at the maximum power point (MPP) and stabilized with a PCE of 20.69% under 1 sun illumination (**Fig. 3d**). It was closed to the PCE value obtained from the *J-V* curve and demonstrated high reliability. Moreover, the external quantum efficiency (EQE) of reference and 10% Gua based PVSCs are measured (**Fig. S10**). A J_{sc} of 22.25 mA cm^{-2} and 22.60 mA cm^{-2} was integrated from EQE spectrum of reference and CsGuaFAMA, respectively, which are well-matched with the values extracted from *J-V* curves. The statistics of photovoltaic parameters obtained from the devices are shown in **Fig. S11** and it is clear that the most obvious impact of the Gua passivation is the enhancement of V_{oc}.

To quantitatively analyse the $V_{oc,\ loss}$ from nonradiative recombination in PVSCs, we describe V_{oc} by several terms related to losses from the ideal V_{oc}, as shown in Equation 1:

$$V_{OC} = V_{oc}^{SQ} + \Delta V_{oc}^{SC} + \Delta V_{oc}^{rad} + \Delta V_{oc}^{nonrad} \quad (1)$$

where ΔV_{oc}^{SC} was the loss from less-than ideal above bandgap J_{SC}, ΔV_{oc}^{rad} can be ascribed to nonideal radiative V_{oc} loss and ΔV_{oc}^{nonrad} was resulted from nonradiative recombination, which are calculated according to the previous works (see ESI† for details) and summarized in **Table S4**. The obtained ΔV_{oc}^{rad} of 5.42 mV for CsGuaFAMA was evidently lower than that of the reference device (29.78 mV), suggesting the lower degree of energy disorder at the band edge. More importantly, we found that the ΔV_{oc}^{nonrad} of CsGuaFAMA is merely 137.03 mV, whereas it is as high as 201.86 mV for reference device. This difference in ΔV_{oc}^{nonrad} is consistent with the increase of 0.08 V in V_{oc}, therefore, we can attribute the low voltage loss for CsGuaFAMA to the suppressed trap-mediated nonradiative recombination. Electrochemical impedance spectroscopy (EIS) was also applied to characterize the charge transport dynamics in solar cells.

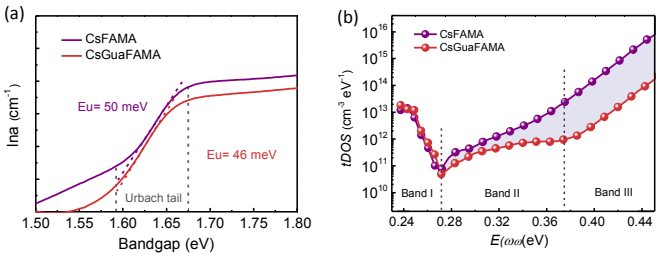

Fig. 4 (a) Plot of ln(α) vs *E* (*hν*) used to extract the Urbach energy of perovskite films with or without Gua and (b) calculated trap density of states.

Fig. S12 showed the Nyquist plots of the devices with 0% and 10% of Gua, which were measured under dark conditions with the frequency range from 500 mHz to 1 MHz and the equivalent circuit is shown in the inset of **Fig. S12**. The series resistance (R_s) is calculated from the Nyquist spectra and it is 23.03 and 16.38 Ω for reference and 10% Gua based device, respectively. Clearly, CsGuaFAMA device exhibited lower R_s and larger R_{rec} values compared to reference device, indicating the better transporting and less charge recombination rate, which further explain the enhanced FF and V_{oc}.

In order to examine the trap states and get more insight into the optoelectronic properties of our prepared perovskite films, we also investigated the Urbach energy (E_u). In the case of reference, the E_u was calculated to be 50 meV while it decreased to 46 meV with the addition of 10% Gua (**Fig. 4a**), which was likely due to the lower band edge disorder and defect density. To characterize both shallow and deep trap states (N_T) and quantize the reduction of N_T, it is calculated from admittance spectroscopy (calculation details are provided in the ESI†) as shown in Fig. 4b and Fig. S13. In the shallow band region (Band I, 0.26-0.27 eV), the N_T of reference device was almost the same with that of CsGuaFAMA. Nevertheless, it was gradually decreased for CsGuaFAMA sample in the deeper region (Band II, 0.27-0.38 eV) and maintained a stable gap in Band III (0.38-0.45 eV), indicating the effective passivation of defects in deep band region.

In summary, we have comprehensively studied the structural, photophysical, photovoltaic properties of new perovskite compositions based on CsGuaFAMA mixed cations. It is found that the defects are effectively passivated after incorporating Gua, which was verified from the much longer PL lifetime, lower energy disorder in the band edge (Urbach tail), larger charge recombination resistance, and an order of magnitude lower trap state density. These beneficial effects result in a remarkably enhanced V_{oc} from 1.11 V to 1.19 V and an impressive PCE > 21%. Our work highlights the great potential of A-site composition engineering by Gua to reduce the nonradiative recombination centres, which should be highly applicable to other perovskite-based optoelectronic devices.

Conflicts of interest

There are no conflicts to declare.

Acknowledgements

The work was supported by the New Faculty Start-up Grant of the City University of Hong Kong (9610421, 7200587), Department of Energy SunShot (DE-EE 0006710) and the Office of Naval Research (N00014-17-1-2201).

Notes and references

1. Z. Wang, Q. Lin, F. P. Chmiel, N. Sakai, L. M. Herz and H. J. Snaith, *Nat. Energy*, 2017, **2**, 17135.
2. E. H. Anaraki, A. Kermanpur, L. Steier, K. Domanski, T. Matsui, W. Tress, M. Saliba, A. Abate, M. Grätzel, A. Hagfeldt and J.-P. Correa-Baena, *Energy & Environmental Science*, 2016, **9**, 3128.
3. NREL efficiency chart. https://www.nrel.gov/pv/assets/pdfs/pv-efficiency-chart.20181221.pdf (accessed Dec 28, 2018).
4. S. D. Stranks, *ACS Energy Lett.*, 2017, **2**, 1515.
5. X. Li, C.-C. Chen, M. Cai, X. Hua, F. Xie, X. Liu, J. Hua, Y.-T. Long, H. Tian and L. Han, *Adv. Energy Mater.*, 2018, **8**, 1800715.
6. Y. Cho, A. M. Soufiani, J. S. Yun, J. Kim, D. S. Lee, J. Seidel, X. Deng, M. A. Green, S. Huang and A. W. Y. Ho-Baillie, *Adv. Energy Mater.*, 2018, **8**, 1703392.
7. F. Zhang, W. Shi, J. Luo, N. Pellet, C. Yi, X. Li, X. Zhao, T. J. S. Dennis, X. Li, S. Wang, Y. Xiao, S. M. Zakeeruddin, D. Bi and M. Grätzel, *Adv. Mater.*, 2017, **29**, 1606806.
8. F. Fu, S. Pisoni, T. P. Weiss, T. Feurer, A. Wäckerlin, P. Fuchs, S. Nishiwaki, L. Zortea, A. N. Tiwari and S. Buecheler, *Adv Sci*, 2018, **5**, 1700675.
9. A. Rajagopal, P.-W. Liang, C.-C. Chueh, Z. Yang and A. K. Y. Jen, *ACS Energy Lett.*, 2017, **2**, 2531.
10. M. Saliba, T. Matsui, K. Domanski, J.-Y. Seo, A. Ummadisingu, S. M. Zakeeruddin, J.-P. Correa-Baena, W. R. Tress, A. Abate, A. Hagfeldt and M. Grätzel, *Science*, 2016, **354**, 206.
11. D.-Y. Son, S.-G. Kim, J.-Y. Seo, S.-H. Lee, H. Shin, D. Lee and N.-G. Park, *J. Am. Chem. Soc.*, 2018, **140**, 1358.
12. C. Ran, J. Xi, W. Gao, F. Yuan, T. Lei, B. Jiao, X. Hou and Z. Wu, *ACS Energy Lett.*, 2018, **3**, 713.
13. K. T. Cho, G. Grancini, Y. Lee, E. Oveisi, J. Ryu, O. Almora, M. Tschumi, P. A. Schouwink, G. Seo, S. Heo, J. Park, J. Jang, S. Paek, G. Garcia-Belmonte and M. K. Nazeeruddin, *Energy Environ. Sci.*, 2018, **11**, 952.
14. Y. Bai, S. Xiao, C. Hu, T. Zhang, X. Meng, H. Lin, Y. Yang and S. Yang, *Adv. Energy Mater.*, 2017, **7**, 1701038.
15. Y. Lin, Y. Bai, Y. Fang, Z. Chen, S. Yang, X. Zheng, S. Tang, Y. Liu, J. Zhao and J. Huang, *J Phys Chem Lett*, 2018, **9**, 654.
16. N. De Marco, H. Zhou, Q. Chen, P. Sun, Z. Liu, L. Meng, E.-P. Yao, Y. Liu, A. Schiffer and Y. Yang, *Nano Lett.*, 2016, **16**, 1009.
17. D. J. Kubicki, D. Prochowicz, A. Hofstetter, M. Saski, P. Yadav, D. Bi, N. Pellet, J. Lewiński, S. M. Zakeeruddin, M. Grätzel and L. Emsley, *J. Am. Chem. Soc.*, 2018, **140**, 3345.
18. A. D. Jodlowski, C. Roldán-Carmona, G. Grancini, M. Salado, M. Ralaiarisoa, S. Ahmad, N. Koch, L. Camacho, G. de Miguel and M. K. Nazeeruddin, *Nat. Energy*, 2017, **2**, 972.
19. R. J. Stoddard, A. Rajagopal, R. L. Palmer, I. L. Braly, A. K. Y. Jen and H. W. Hillhouse, *ACS Energy Lett.*, 2018, **3**, 1261.
20. N. D. Pham, C. Zhang, V. T. Tiong, S. Zhang, G. Will, A. Bou, J. Bisquert, P. E. Shaw, A. Du, G. J. Wilson and H. Wang, *Adv. Funct. Mater.*, 2019, **29**, 1806479.
21. A. D. Jodlowski, A. Yépez, R. Luque, L. Camacho and G. de Miguel, *Energy Environ. Sci.*, 2016, **55**, 14972.
22. J. Yuan, X. Ling, D. Yang, F. Li, S. Zhou, J. Shi, Y. Qian, J. Hu, Y. Sun, Y. Yang, X. Gao, S. Duhm, Q. Zhang and W. Ma, *Joule*, 2018, **2**, 2450.
23. D. J. Slotcavage, H. I. Karunadasa and M. D. McGehee, *ACS Energy Lett.*, 2016, **1**, 1199.
24. D. W. de Quilettes, S. M. Vorpahl, S. D. Stranks, H. Nagaoka, G. E. Eperon, M. E. Ziffer, H. J. Snaith and D. S. Ginger, *Science*, 2015, **348**, 683.